Journal of Sound and Vibration (1999) **226**(5), 905–922
Article No. jsvi.1999.2323, available online at http://www.idealibrary.com on IDEAL®

ADAPTIVE FINITE ELEMENT STRATEGY FOR ACOUSTIC PROBLEMS

R. BAUŠYS† AND N.-E. WIBERG

Department of Structural Mechanics, Chalmers University of Technology, Sven Hultinsgata 8, *SE*-41296 *Göteborg, Sweden*

(*Received* 16 *September* 1998, *and in final form* 15 *March* 1999)

A *h*-adaptive finite element strategy for acoustic problems is presented. The key features of the strategy are error estimation, adaptive mesh generation and remeshing, finite element analysis. The error estimation has been performed using the superconvergent patch recovery technique for prime variables of finite element approximation (SPRD). For adaptive mesh generation and remeshing, the commercial software package I-DEAS has been applied. Finite element analysis has been performed using commercial software package SYSNOISE. Numerical examples are shown to illustrate the properties of the SPRD technique and the procedure of the proposed adaptive strategy.

1. INTRODUCTION

Most practical problems of acoustics are solved by standard computational techniques such as boundary element method (BEM), finite difference and finite element method (FEM). The finite element method can be preferred to the boundary element technique due to the fact that FEM does not encounter the difficulties of numerical implementation which are common for the BEM approach. However, even after more than 30 years of development of the finite element method, the question of estimating and controlling discretization errors remains a major topic of research.

In acoustic problems, steady state sound response is governed by the Helmholtz equation, which can be characterized by a potential loss of ellipticity with increasing wave number in the propagation region. The Galerkin method provides good phase and amplitude accuracy as long as the mesh is fine enough with respect to the wave number. However, "fine enough" is often too expensive for adequate resolution, even for moderate wave numbers. So one of the main concerns in acoustic finite element analysis is the adequacy of the finite element mesh. Acousticians often use the so-called "rule of the thumb" which prescribes the minimal discretization of a wavelength. A non-uniform finite element mesh is needed in many practical problems; increasingly finer grids are required near

† On leave from Department of Engineering Mechanics, Vilnius Technical University, LT-2040 Vilnius, Lithuania.

0022-460X/99/400905 + 18 $30.00/0

singularities and non-smooth boundaries. Such a discretization process, which is based on the "rule of thumb", is unable to predict a proper resolution and the proper order of the approximation at each location and usually produces a mesh with too many elements and still one does not have a direct measure of the error. Another alternative is to find some means to identify critical regions that have to be refined. That is, starting solving problems on a crude mesh, one has to estimate truncation errors in different locations.

The most popular approach to enhance accuracy in an efficient way is to use an adaptive finite element strategy. In recent years, many adaptive methods have been proposed using different error estimators that can greatly improve the quality of the finite element solution. In particular, the *h*-method is widely applied, where the new degrees of freedom have to be added to the selected elements in the analysis domain by the subdivision of elements or by a completely new unstructured mesh.

The most important ingredient in an adaptive remeshing approach is the highly reliable estimation of the discretization errors. *A posteriori* error estimation continues to be an active research area since the past decade. Some *a posteriori* error estimators have been proposed recently. Bouillard *et al.* [1] implemented the original superconvergent patch recovery (SPR) technique for acoustic finite element analysis. The original concepts are extended to complex variables and the reliability of the error estimation is studied. Tetambe and Rajakumar [2] presented the error estimation strategy for acoustic analysis based on nodal averaging technique. A residual-based *a posteriori* error estimator for Helmholtz equation was presented by Harari *et al.* [3].

In the present study, we have implemented the superconvergent patch recovery for prime variables (SPRD) technique to estimate the discretization error of the solution. Originally, this technique was proposed to assess the quality of the finite element solution in free vibration analysis [4, 5].

Nowadays, in many commercial software packages, error estimation techniques are mainly available for linear structural and steady state thermal analyses. Since commercial software for finite element analysis provides many features for interfacing with other mechanical computer-aided engineering technologies, we construct an adaptive remeshing strategy combining our error estimation technique with the available commercial packages. For finite element analysis we use the commercial code SYSNOISE [6]. The commercial package I-DEAS [7] is implemented to generate the initial mesh and to perform adaptive remeshing procedures. The numerical methods used in the technique are outlined and several examples are cited to show the wide range of this method's applicability. In the following sections, we present the development and implementation of our approach with its main issues: mesh generator, solution procedure, error estimator and refinement strategy.

2. ERROR ESTIMATION

In adaptive analysis the error estimate plays a crucial role, which not only provides the information about the accuracy of the finite element solution, but also gives the indicator for mesh refinement.

At the beginning we present governing equations of the acoustical analysis. The wave equation governing the propagation of sound through as a compressible, inviscid, non-flowing fluid in enclosures can be concisely expressed as [8]

$$\nabla^2 p - \frac{1}{c^2}\frac{\partial^2 p}{\partial t^2} = 0 \tag{1}$$

with boundary conditions

$$p = p_e \quad \text{on } S_1, \tag{2}$$

$$\frac{1}{\rho}\nabla p \cdot \mathbf{n} = -\frac{\partial v}{\partial t} \quad \text{on } S_2, \frac{1}{\rho}\nabla p \cdot \mathbf{n} = -\frac{1}{Z_a}\frac{\partial p}{\partial t} \quad \text{on } S_3, \tag{3,4}$$

where ∇^2 is the Laplacian operator, p is the acoustical pressure, c is the sound speed, v is the fluid particle velocity, ρ is the density of the fluid, $\mathbf{n}$ is a unit normal to S_2 and Z_a is the normal acoustic impedance, S_1, S_2, S_3 denote the boundaries with Dirichlet, Neumann and Robin conditions respectively. It is assumed that acoustic pressure is a time harmonic function $p = q e^{j\omega t}$. With finite element approximation $q^h = \mathbf{N}(x)\mathbf{q}$, using standard Galerkin procedure, the governing equations for the frequency domain will be of the form

$$(\mathbf{K} + j\rho\omega\mathbf{C} - \omega^2\mathbf{M})\mathbf{q} = -j\rho\omega\mathbf{F}, \tag{5}$$

where $\mathbf{K}$ is derived from the fluid potential energy; $\mathbf{C}$ is derived from the energy dissipated on the boundary walls and $\mathbf{M}$ is derived by using the kinetic energy expression, ω is the angular frequency of excitation, $\mathbf{F}$ is the generalized excitation term and $\mathbf{q}$ is the vector of nodal pressure values.

With the finite element solution of the problem, pressure and velocity approximations q^h and $v^h = -(1/j\rho\omega)\nabla q^h$, respectively, are obtained. To calculate steady state pressure and velocities the commercial SYSNOISE code is employed.

In order to measure accuracy one has to introduce suitable norms. The error of the finite element solution can be defined by using the usual H^1-seminorm

$$|e|_1^2 = \int_\Omega (v^{\mathrm{T}} - v_h^{\mathrm{T}})(\tilde{v} - \tilde{v}_h)\,\mathrm{d}\Omega, \tag{6}$$

where v is the exact solution for the velocities, Ω denotes the fluid domain and $\tilde{\bullet}$ denotes the complex conjugate. A relative error of the finite element approximation can be expressed as

$$\eta = |e|_1/|q|_1 \quad \text{with} \quad |q|_1^2 = \int_\Omega v^{\mathrm{T}}\tilde{v}\,\mathrm{d}\Omega. \tag{7}$$

From *a priori* error estimation results [9], one can express that the global relative error is bounded as

$$\eta \leqslant C_1(m)\theta^m + C_2(m)k\theta^{2m}, \tag{8}$$

with $\theta = kh/2m$, wave number $k = \omega/c$, where m is the order of the FE basis functions and h is the characteristic size of the finite elements. For linear elements

$m = 1$, equation (8) will be of the form

$$n \leqslant C_1 kh + C_2 k^3 h^2. \tag{9}$$

The first term in the error bound reflects the classical best approximation error while the second term indicates pollution of optimal error for high wave number [9].

As the exact solution of the problem generally is not known, the errors are usually estimated by *a posteriori* methods. There have been a number of methods to estimate the discretization error of the finite element solution. One of the most popular approaches is the so-called postprocessed error estimator. The purpose of the postprocessed error estimation is to provide a local estimate of the solution error in some norm. Subsequent to the determination of the improved pressure field the elementwise and the global errors are computed. In the postprocessed procedures the errors are estimated by computing the difference between an improved solution and the original finite element solution as follows:

$$|\bar{e}|_1^2 = \int_\Omega (v^{*\mathrm{T}} - v_h^{\mathrm{T}})(\tilde{v}^* - \tilde{v}_h)\,\mathrm{d}\Omega. \tag{10}$$

The improved velocity solution v^* is determined from the new pressure field q^* of higher order of accuracy, which is obtained by using the SPRD technique.

This new pressure field q^* of $m + 1$ order will be defined over a patch of elements and this new field is required to be a least-squares fit to the original finite element solution at the superconvergent points where the accuracy of the finite element solution is higher. These locations for prime variables of the finite element approximation are nodal points. The new pressure field q^* over an element is constructed by using ordinary local basis functions of the order $m + 1$,

$$q^*(x) = \sum_r \mathbf{N}(\mathbf{x})_r^* (\mathbf{q}_r^*) + \sum_s \mathbf{N}(\mathbf{x})_s^* (\mathbf{q}_s^*), \tag{11}$$

where r is used to denote the original finite element nodes and s denotes the additional nodes of the element of the recovered displacement field; $\mathbf{N}_r^*(\mathbf{x})$ and $\mathbf{N}_s^*(\mathbf{x})$ are the local basis functions of the order $m + 1$ associated with the original element nodes and the additional ones respectively.

The nodal values of the original finite element pressures are assumed to be the same as those of the original finite element solution $\mathbf{q}_q^* \equiv \mathbf{q}_r^h$, and the recovered pressure values $\mathbf{q}_s^*$ at the additional nodes are obtained by solving the following least-squares problem in the element patch.

Find $\mathbf{q}^* \in P_{m+1}$ such that

$$J_{\Omega_t}(\mathbf{q}^*) = \min_{q^{f*} \in P_{m+1}} J_{\Omega_t}(\mathbf{q}^{f*}), \tag{12}$$

where

$$J_{\Omega_t}(\mathbf{q}^{f*}) = \sum_{j=1}^{ns} w_j^2 \mathbf{R}_q^{\mathrm{T}}(\mathbf{x}_j)\mathbf{R}_q(\mathbf{x}_j), \tag{13}$$

in which the residual $R_q(x_j)$ is calculated at the locations ns where the original finite element solution is superconvergent or at least highly accurate (nodal points), w_j denotes the weighting function (for more details see [4]) and Ω_t denotes the domain of the element patch. The residual is defined by

$$\mathbf{R}_q = \mathbf{q}^{f*} - \mathbf{q}^h, \tag{14}$$

and $\mathbf{q}^{f*}$ belongs to a polynomial expansion of order $m + 1$,

$$\mathbf{q}^{f*} = \mathbf{Q}(\mathbf{x})\mathbf{b}, \tag{15}$$

where $\mathbf{Q}(\mathbf{x})$ is a row matrix containing a monomial term of physical co-ordinates of $m + 1$ order, and the vector $\mathbf{b}$ is a set of unknown parameters to be determined.

We use a reduced element patch described in reference [4] which has an extension of size $2h$ (where h is a characteristic element size in the local patch) in order to maintain the locality of the least-squares fit. This enables us to reduce the cost of computation and at the same time to increase the accuracy of the recovered displacement field. Only boundary patches, which have not enough elements for a reduced patch, are constructed in the usual way.

The approach described is a local updating method, so no global system of the equations has to be solved. The number of equations to be solved is small and the cost of the recovery procedure is proportional to the number of the mesh nodes.

The quality of the error estimator is measured by its effectivity index, defined as the ratio between the estimated and the exact errors:

$$\theta = |\bar{e}|/|e|. \tag{16}$$

An error estimator is named asymptotically exact if θ approaches unity as the characteristic size of the finite element h tends to zero.

With the estimated error in each element at hand, the total error of the finite element solution becomes

$$|\bar{e}|^2 = \sum_{i=1}^{NEL} |\bar{e}_i|^2, \tag{17}$$

where NEL is the total number of elements. As the estimated error is calculated for each element, it can be used to determine portions of the finite element mesh which need to be refined.

3. REMESHING STRATEGY

In this section we present a method with a global remeshing strategy which provides a very simple and rapid way to perform adaptive computations. The main ingredients of this remeshing strategy are ***h*-refinement**—consists on building a new mesh, using the same type of elements; **optimality criteria**—refinement is organized with the aim of achieving equal error in each element of the new mesh; **iterative process**—the target in each stage of refinement is to reduce the global error until the calculated error drops below a users specified value.

The main goal of this strategy is to obtain the refined mesh, which has an acceptable error level for the whole domain, and this can be stated as

$$\eta^h \leqslant \bar{\eta}, \tag{18}$$

where $\bar{\eta}$ is the maximum permissible error. To obtain the mesh which satisfies this condition, we implement the standard h-method which is based on the consideration that the discretization error is constant in the element. The overall accuracy of the numerical simulation is measured through the non-dimensional estimated global error, which may be regarded as a sum of the element contributions,

$$\eta^h = \sqrt{\sum_{e=1}^{NEL} \eta_e^2}, \quad \eta_e = |\bar{e}|_e / \sqrt{|q^h|^2 + |\bar{e}|^2}, \tag{19}$$

where $|q^h|$ denotes the seminorm of the FE solution itself. The accuracy of the numerical simulation can be measured through the other acoustic global indicators.

Once error estimation has been performed and global error does not satisfy the prescribed tolerance, the next step is to refine the mesh. The remeshing process is driven by the estimated relative element errors. These estimated relative element errors η_e are used as the initial information for adaptive remeshing within I-DEAS. The new element sizes are calculated by the use of a mesh optimality criterion to be an equally distributed error over the elements.

The flowchart of a generic adaptive strategy is shown in Figure 1.

4. NUMERICAL EXAMPLES

Numerical examples from 2-D acoustics will demonstrate the performances of the SPRD technique for the error estimation and adaptive remeshing strategy. As it was mentioned above, the recovered pressure field $\mathbf{q}^*$ is constructed by using $\mathbf{Q}(\mathbf{x})$ with a polynomial of order $m + 1$ for all quadrilateral and triangular elements. For all examples, fluid properties with sound velocity $c = 340$ m/s and density ρ set to 1·225 kg/m^3 are assumed. An acoustic excitation is caused by a piston-like surface under harmonic motion at a velocity amplitude of v_0 along the normal to the surface. Adaptive remeshing strategy is performed by using 3-node linear triangular elements.

4.1. TUBE PROBLEM

Consider a tube of length $L = 1{\cdot}0$ m and width $H = 0{\cdot}1$ m which is shown in Figure 2. The surface of the excitation is at the left end of the tube. On the other boundaries the normal velocity is set to zero. Regular meshes for both elements linear, quadrilateral and triangular, are considered. Typical meshes for quadrilateral and triangular elements are presented in Figures 2 and 3. A sequence of three regular meshes with 20×2, 40×4 and 80×8 elements is used to study the rate of convergence and the accuracy of the results for both quadrilateral and triangular elements.

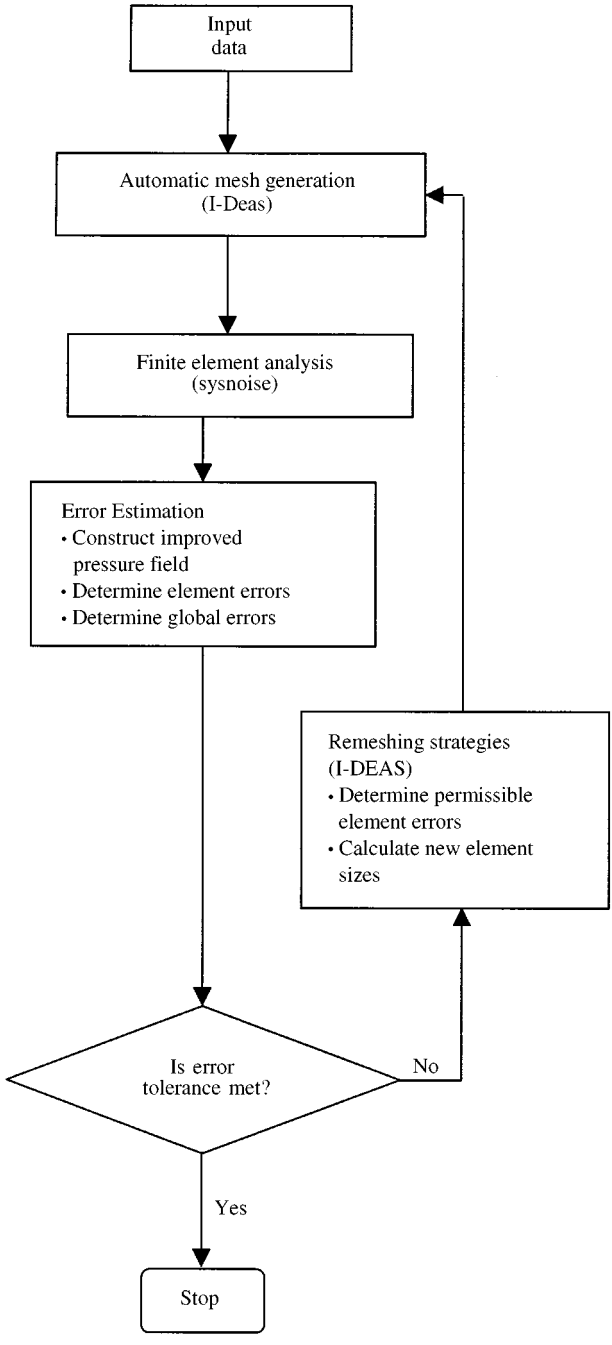

Figure 1. Flow chart of the adaptive acoustic analysis.

For this problem an analytical solution is available and can be expressed by

$$v(x) = \frac{v_0}{\sin(kL)} \sin[k(L - x)]. \tag{20}$$

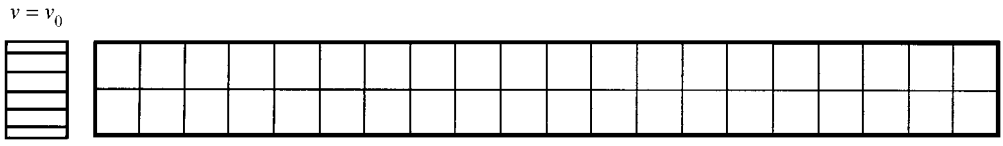

Figure 2. Geometry, excitation and typical quadrilateral mesh.

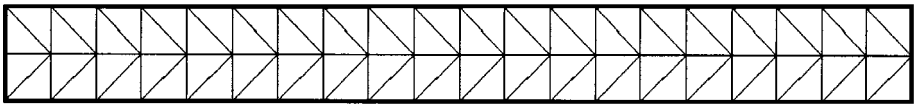

Figure 3. Typical triangular mesh.

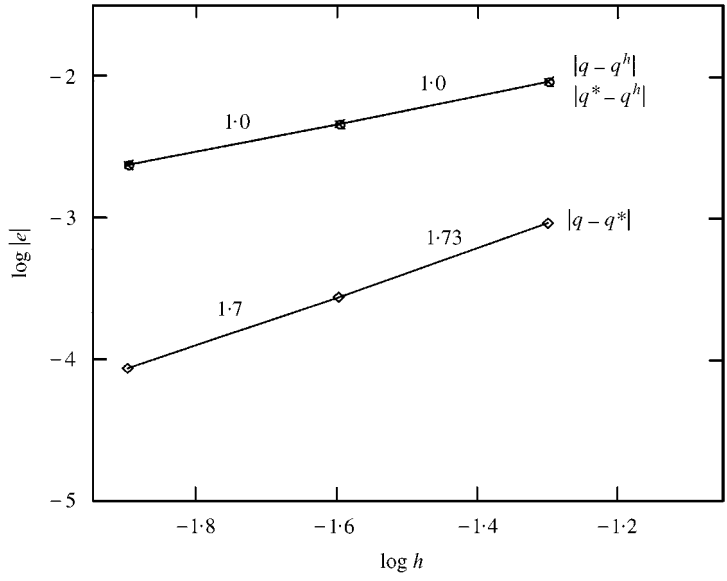

Figure 4. Convergence rate of triangular elements at 50 Hz.

The error estimation was performed for two frequencies of the excitation, 50 and 750 Hz. In the first case, the non-dimensional wave number k' is then equal to 0·92 and for the coarsest mesh $kh = 0{\cdot}046 \ll 1$ and $k^2h = 0{\cdot}0432 \ll 1$ and we will study the behaviour of the postprocessed error estimation in the asymptotic range since both assumptions concerning kh and k^2h hold. In the second case k' is equal to 13·85 and for the coarsest mesh $kh = 0{\cdot}691 < 1$ and $k^2h = 9{\cdot}59 > 1$ and we will study the behaviour of the postprocessed error estimation in the preasymptotic range since only the assumption concerning kh holds. Notice that only in the first case does the non-dimensional wave number respects the criterion of low wave number. The numerical results of the convergence rate for linear triangular elements are plotted in Figures 4 and 5. The error in energy norm of the original finite element solution $|q - q^h|$, of the post-processed solution $|q^* - q^h|$ and of the estimated error of the

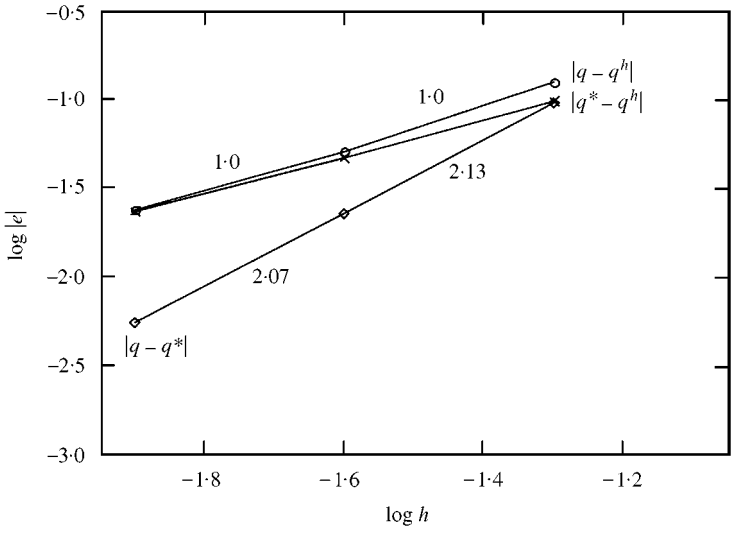

Figure 5. Convergence rate of triangular elements at 750 Hz.

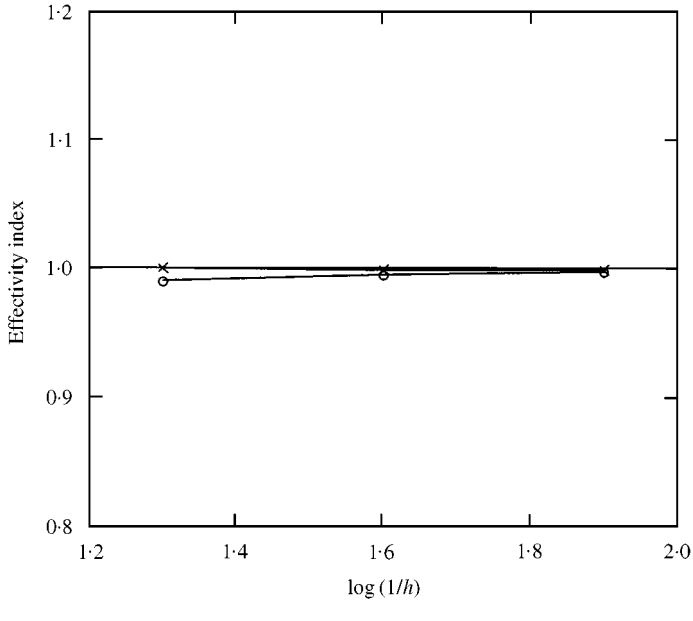

Figure 6. Effectivity indices of triangular and quadrilateral elements of 50 Hz.

finite element solution $|q - q^*|$ is presented in these figures. With the results of the numerical experiments at hand, one can make the following observations.

1. The original finite element solution exhibits order of accuracy O(h) as predicted by *a priori* error estimation.
2. The recovered solution obtained by SPRD technique demonstrates superior accuracy with respect to the original finite element solution.

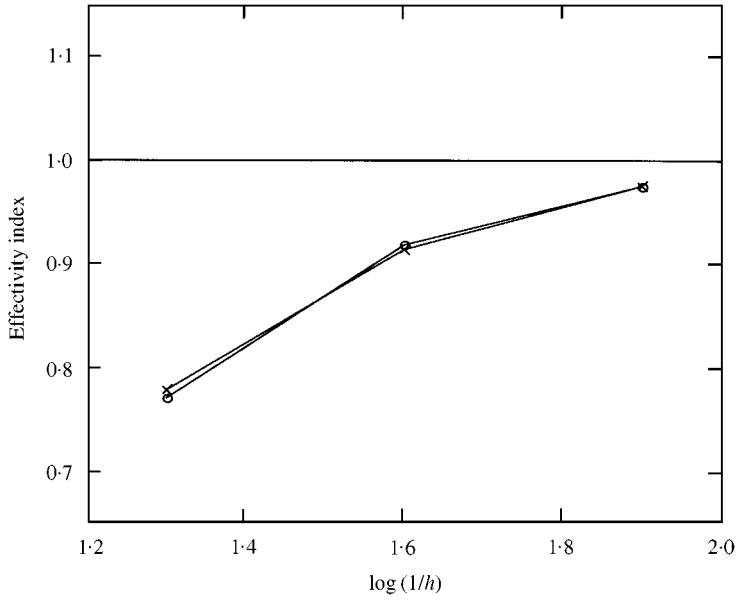

Figure 7. Effectivity indices of triangular and quadrilateral elements at 750 Hz.

3. The superconvergent properties of the improved solution are demonstrated for both cases in asymptotic and preasymptotic ranges.
4. The proposed SPRD technique slightly underestimates the exact error of the finite element solution.

The convergence of the effectivity indices is plotted in Figures 6 and 7. One can observe that the effectivity indices converge to one rapidly for both the quadrilateral and triangular elements tested when the finite element mesh is refined. The numerical results show an asymptotic exactness of the proposed error estimator based on the SPRD technique.

4.2. TWO-DIMENSIONAL CAVITY

The second example is a room of length $L = 5$ m and width $H = 3$ m as shown in Figure 8. Acoustic excitation is presented by a vibrating panel with velocity $v_0 = 1{\cdot}0$ m/s as shown in the figure. The normal boundary velocity is set to be 0 at the other sides. The first five acoustic eigenfrequencies obtained by the initial mesh are as follows: 34·15, 57·16, 66·9, 69·18 and 90·73 Hz. Two different frequencies of excitation 20 and 190 Hz are studied. The sequence of adaptive remeshing begins with quite coarse mesh of 127 elements and results in a solution in which the relative error is 26·1% at 20 Hz and 33·1% at 190 Hz. The final meshes, which are obtained after four steps, are presented in Figures 9 and 10. Trying to obtain a final mesh in a single adaptive step would result in the over-refinement of the mesh. It is apparent that at low frequencies the improvement is very local and at the higher

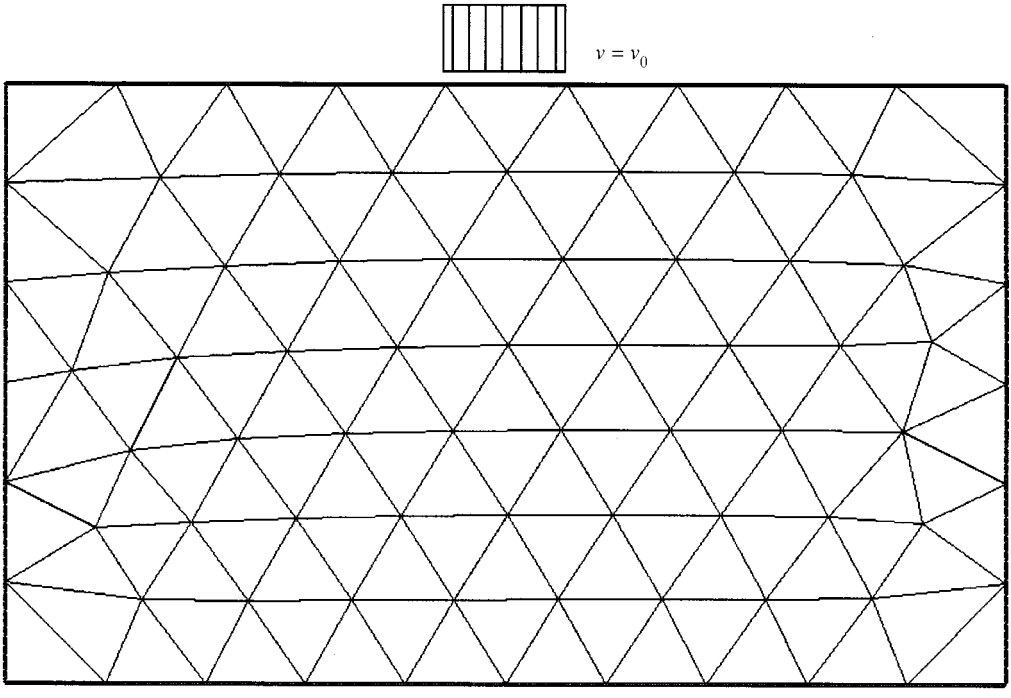

Figure 8. Geometry, boundary conditions and initial mesh of the room.

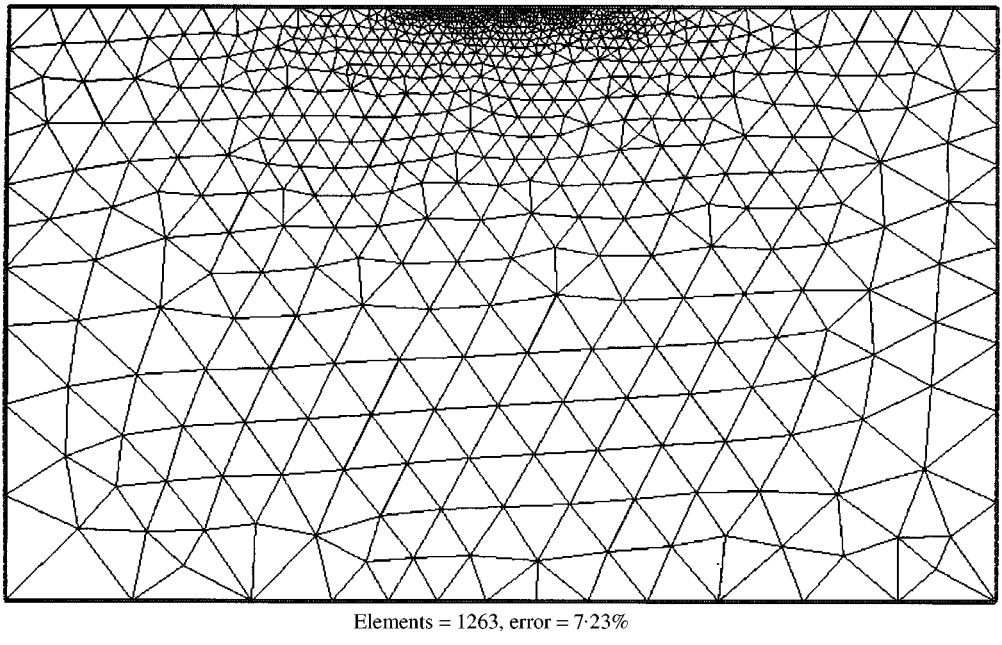

Figure 9. Final mesh of the room at 20 Hz.

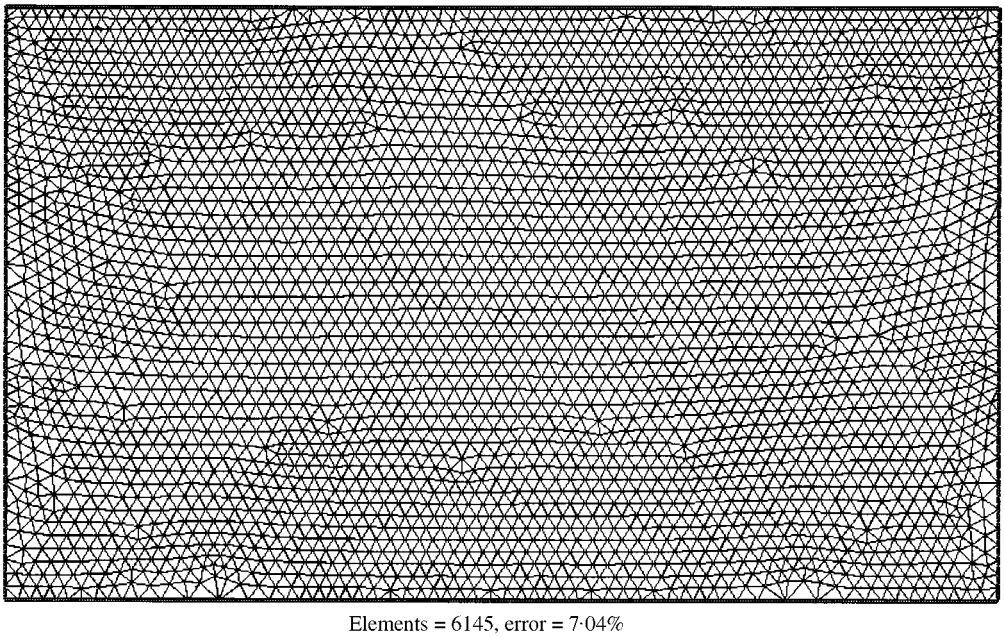

Elements = 6145, error = 7·04%

Figure 10. Final mesh of the room at 190 Hz.

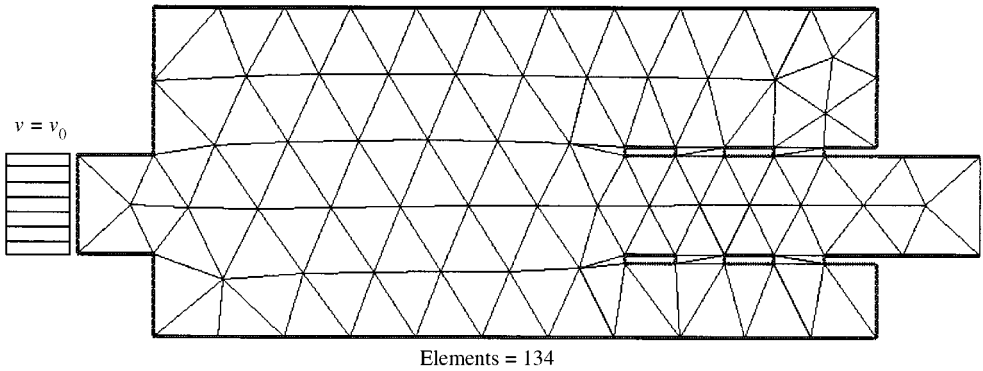

Elements = 134

Figure 11. Geometry, boundary conditions and initial mesh of expansion chamber.

frequencies one has a demand for refinement in all the cavity. It should be mentioned that **no** *a priori* information is used to achieve the solution of the required accuracy.

4.3. EXPANSION CHAMBER

The two-dimensional model of the expansion chamber with a perforated outlet pipe studied as shown in Figure 11. Acoustic excitation is presented by a vibrating

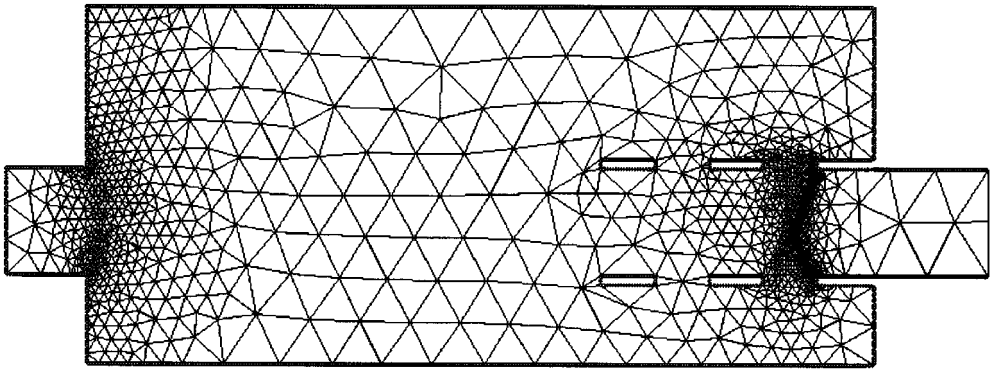

Figure 12. Optimal mesh of the expansion chamber at 100 Hz.

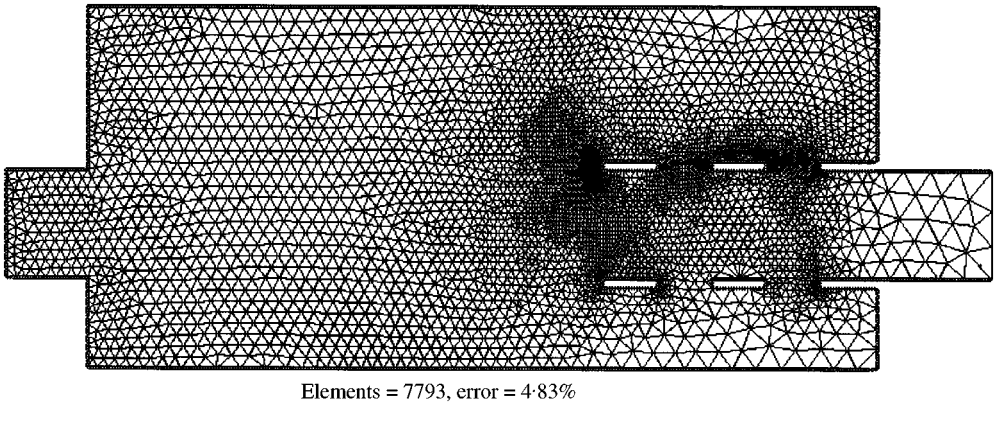

Figure 13. Optimal mesh of the expansion chamber at 1100 Hz.

panel with velocity $v_0 = 0{\cdot}1$ ms at the left-hand side. At the right-hand side the boundary condition of the form $\partial q/\partial n = \mathrm{j}kq$, equation (4), is assumed. The normal boundary velocity is set to be 0 at the other sides. The first five acoustic eigenfrequencies obtained by the initial mesh are as follows: 360·77, 687·09, 826·66, 897·11 and 1130·16 Hz. Two different frequencies of excitation, 100 and 1100 Hz, are studied. The adaptive remeshing procedure starts with an initial mesh of 134 elements and relative errors of the finite element solution are 21·97% at 100 Hz and 23·09% at 1100 Hz. For both cases the optimal meshes are presented in Figures 12 and 13. The optimal meshes are found after four steps. In the case of the low frequency the optimal mesh in comparison with initial mesh enables one to detect singularities of the finite element solution but the distributions of the main characteristics such as pressure and velocities are quite close outside the regions of singularities. For the higher frequency case the initial and optimal meshes produce completely different fields of the pressure as shown in Figures 14 and 15.

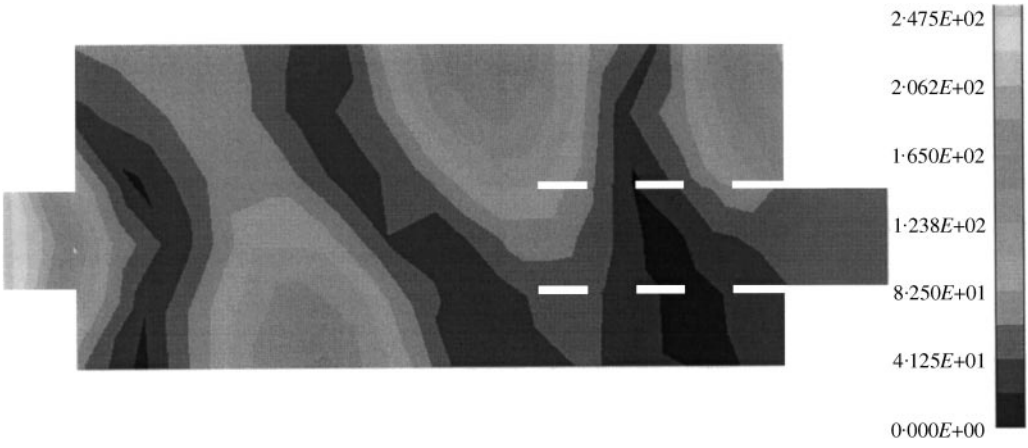

Figure 14. Pressure by initial mesh at 1100 Hz.

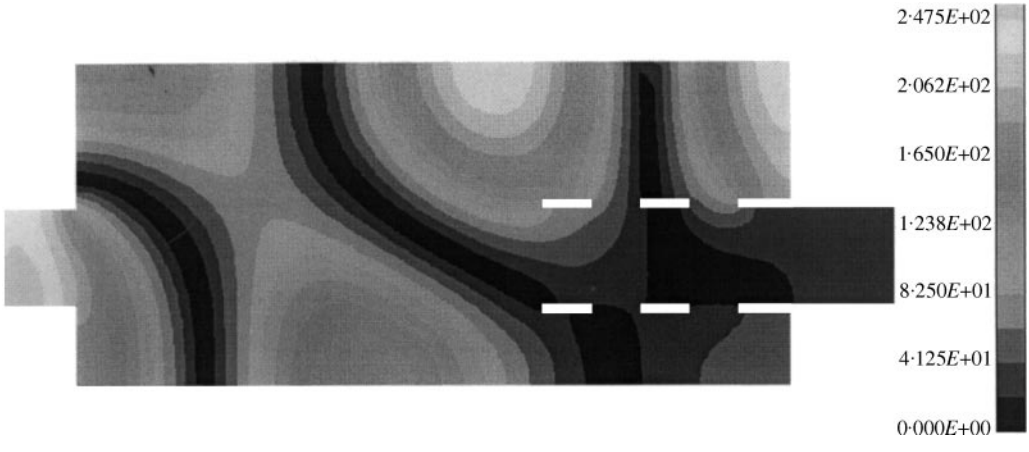

Figure 15. Pressure by optimal mesh at 1100 Hz.

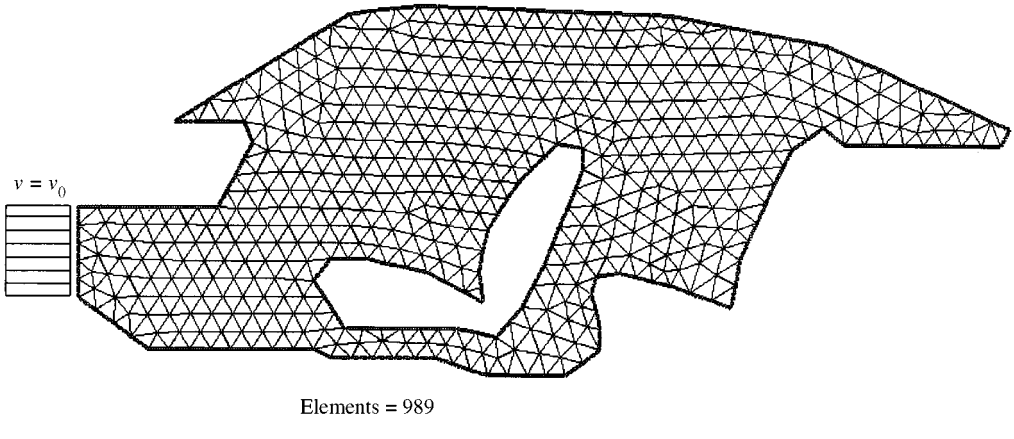

Figure 16. Geometry, boundary conditions and initial mesh of the car enclosure.

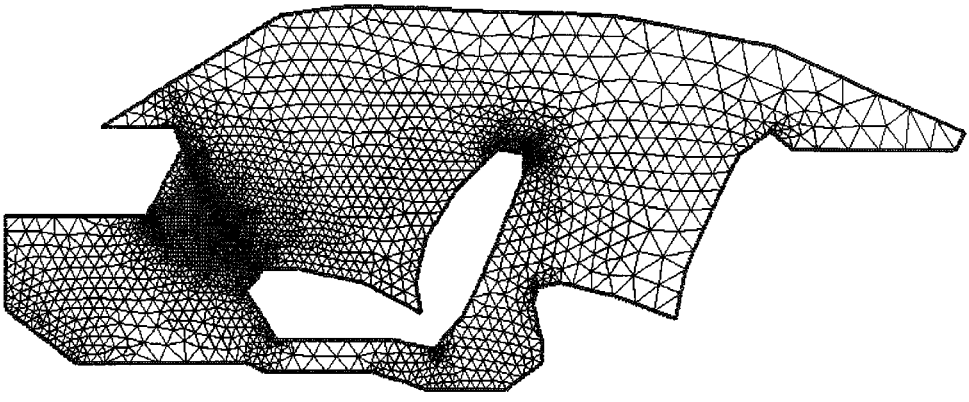

Figure 17. Optimal mesh of the car enclosure at 50 Hz.

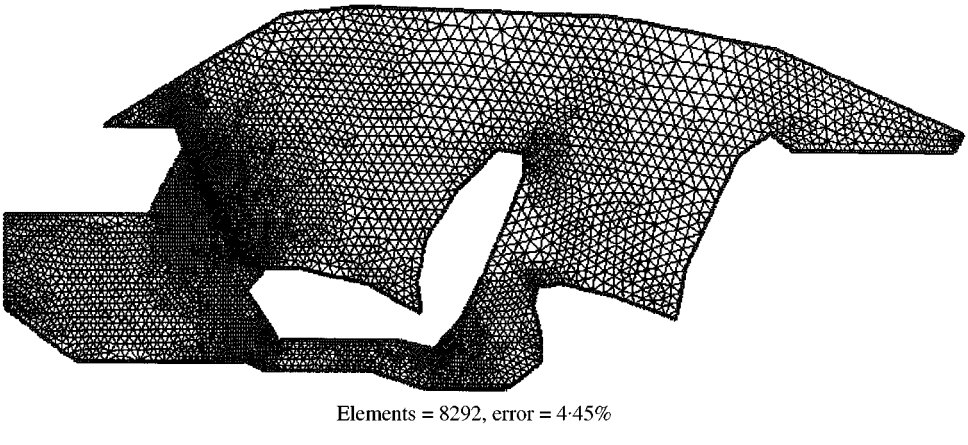

Figure 18. Optimal mesh of the car enclosure at 350 Hz.

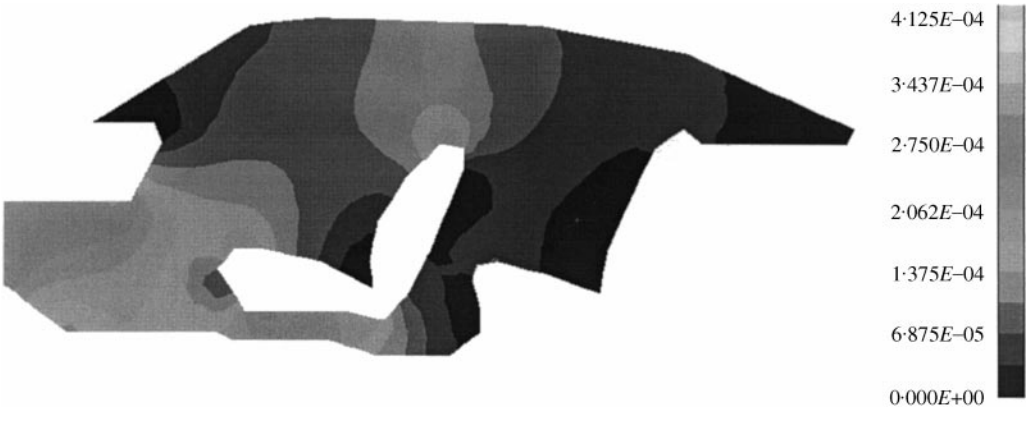

Figure 19. Velocity in car enclosure (x direction/amplitude) at 50 Hz by initial mesh.

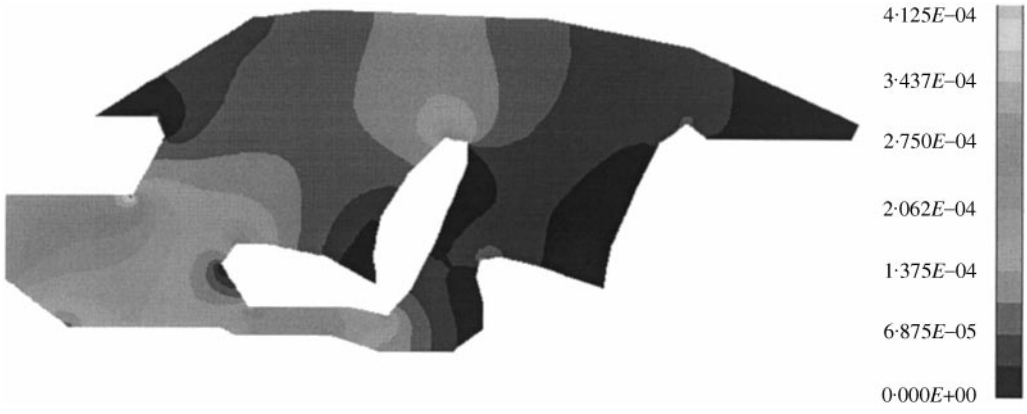

Figure 20. Velocity in car enclosure (x direction/amplitude) at 50 Hz by optimal mesh.

Figure 21. Velocity in car enclosure (x direction/amplitude) at 350 Hz by initial mesh.

4.4. CAR ENCLOSURE

The two-dimensional model of the car enclosure is presented in Figure 16. The normal boundary velocity is set to be 0 at all sides except for the vibrating panel with velocity $v_0 = 3{\cdot}0 \times 10^{-4}$ m/s at the left-hand side. The first five acoustic eigenfrequencies obtained by the initial mesh are as follows: 74·38, 122·33, 131·14, 175·88 and 230·39 Hz. Two different frequencies of excitation, 50 and 350 Hz, are studied. The initial mesh of 989 elements used in the adaptive scheme gives the relative errors of the finite element solution as 7·41% at 50 Hz and 13·27% at 350 Hz. For both cases, the optimal meshes are presented in Figures 17 and 18. It is apparent that at the higher frequency the optimal mesh consists of a larger number of elements but some regions of utmost refinement coincide. The comparison of the velocity in the x direction simulated by the initial and optimal meshes at different frequencies is presented in Figures 19–22. It is evident that in the case of low frequencies of excitation, simulation by the initial mesh does not detect the

Figure 22. Velocity in car enclosure (x direction/amplitude) at 350 Hz by optimal mesh.

singularities of the solution. In the case of higher frequencies simulation by the optimal mesh produces the peaks of the velocity in more local regions.

5. CONCLUSIONS

The paper has presented an adaptive finite element strategy for acoustic problems. This strategy uses adaptive finite element meshing and remeshing that is performed by the commercial package I-DEAS, finite element analysis using the software SYSNOISE and error estimation is done by an additional postprocessing unit. Superconvergent patch recovery technique for prime variables of finite element approximation (SPRD) is applied for the error estimation. Numerical experiments show the reliability of the proposed SPRD technique due to the fact that the recovered gradient field exhibits superconvergence properties. The proposed adaptive strategy is based on h-refinement. Numerical examples have demonstrated that the present adaptive strategy is able to create an optimal mesh in which the criterion of the error equidistribution is satisfied. The designed optimal meshes provide not only solutions of the prescribed accuracy but also detect all singularities in the solution. Although two-dimensional problems are studied, the proposed strategy can be extended to three-dimensional problems.

ACKNOWLEDGMENT

The authors thank Prof. W. Kropp from the Department of Applied Acoustics, Chalmers University of Technology for useful discussions.

REFERENCES

1. Ph.Bouillard, J.-F. Allard and G. Warzee 1996 *Communications in Numerical Methods in Engineering* **12**, 581–594. Superconvergent patch recovery technique for the finite element method in acoustics.

2. R. P. Tetambe and C. Rajakumar 1996 *Computers and Structures* **61**, 13–19. Estimation of error in finite element acoustic analysis.
3. I. Harari, K. Grosh, T. J. R. Hughes, M. Malhotra, P. M. Pinsky, J. R. Stewart and L. L. Thompson 1996 *Archives of Computational Methods in Engineering* **3**, 131–311. Recent development in finite element methods for structural acoustics.
4. N.-E. Wiberg and R. Baušys 1995 *Computing in Civil and Building Engineering* (J. Pal and H. Werner editors), 611–616. Rotterdam, Brookfield: A. A. Balkema. Error estimation for eigenfrequencies and eigenmodes in dynamics.
5. N.-E. Wiberg, R. Baušys and P. Hager 1996 *Advances in Finite Element Technology* (B.H.V. Topping editor), 43–55 Galashiels, Scotland: Civil-Comp Press. Improved eigenfrequencies and eigenmodes in free vibration analysis.
6. Numerical Integration Technologies 1994 *Sysnoise Users Manual*. Sysnoise Rev 5.1, NIT, Ambachtenlaan 11a, 3001 Leuven, Belgium.
7. Structural Dynamics Research Corporation 1996 *I-DEAS Master Series* 3 *Users manual*. SDRC, 2000 Eastman Drive, Milford, OH 45150, US.
8. L. L. Beranek and I. L. Ver 1992 *Noise and Vibration Control Engineering*. New York: Wiley.
9. F. Ihlenburg and I. Babuska 1997 *SIAM Journal of Numerical Analysis* **34**, 315–358. Finite element solution of the Helmholtz equation with high wave number Part II: The *h–p* version of the FEM.